Article

Characteristics and Formation Mechanism of Surface Residual Deformation above Longwall Abandoned Goaf

Erhu Bai [1,2,3,4] , Xueyi Li [2], Wenbing Guo [1,2,3,4], Yi Tan [1,2,3,4,*], Mingjie Guo [2], Peng Wen [2] and Zhibao Ma [2]

1 Shaanxi Provincial Key Laboratory of Geological Support for Coal Green Exploitation, Xi'an University of Science and Technology, Xi'an 710054, China
2 School of Energy Science and Engineering, Henan Polytechnic University, Jiaozuo 454003, China
3 State Key Laboratory of Coal Resources in Western China, Xi'an University of Science and Technology, Xi'an 710054, China
4 State Collaborative Innovative Centre of Coal Work Safety and Clean-Efficiency Utilization, Jiaozuo 454003, China
* Correspondence: tanyi@hpu.edu.cn; Tel.: +86-13453177787

Abstract: With the rapid development of social economy in China, the contradiction between the wide distribution of abandoned goaf and the shortage of land for engineering construction is becoming increasingly prominent. The effective utilization of coal mining subsidence areas has become an effective measure to alleviate the poverty of construction land in mining areas and promote the green transformation of mining cities. The key to the scientific utilization of abandoned goaf is the prevention and control of surface residual deformation, which depends on the formation mechanism of surface residual deformation. Based on the regularity of mining-induced surface movement and deformation under different mining sizes, it is concluded that the full mining degree of working face is the primary condition for entering the surface recession period. The trapezoidal and periodic forward movement characteristics of mining-induced overburden destruction are analyzed. The regularity of upward transmission of mining-induced fissures with overburden destruction is clarified. The influencing factors of surface residual deformation are equivalent to the influencing factors of overburden structure and caved zone. The deformation characteristics of broken rock in the caved zone under different conditions (particle size, gradation, and water content) are analyzed. It is concluded that the surface residual subsidence near the boundary of the goaf is more significant than that in the middle of the goaf. It is revealed that the overburden structure at the boundary of the goaf and the re-compaction of the caved zone is the mechanism of surface residual deformation. The characteristics of surface residual deformation in abandoned goaf have been verified by field measurement, and it is pointed out that the surface residual deformation in abandoned goaf has long-term characteristics, which provides a theoretical basis for accurate prediction of surface residual deformation and rational utilization of abandoned goaf.

Keywords: abandoned goaf; surface residual deformation; formation mechanism; overburden structure

1. Introduction

As an essential fundamental energy source in China, coal occupies a dominant position in China's primary energy structure, accounting for about 60% of said energy structure, and plays an irreplaceable role in developing the national economy [1–3]. According to IHS Markit forecasts, coal will remain the world's most influential power generation energy in the coming decades. When the coal is mined underground, the relative equilibrium strata are disturbed by mining and cause movement, deformation and destruction. As the coal mining continues, the influence range will be expanded continuously, and transmitted upward to the surface, forming a much larger subsidence basin than the goaf. Due to the hysteresis of surface subsidence, the surface subsidence will continue for a period of

time after the working face completed, thus forming the final surface movement basin. Therefore, the geological and environmental problems have been caused by large-scale coal mining, such as surface subsidence, landslide, groundwater loss, land desertification, and vegetation destruction [4–9], have seriously restricted the regional economic development, social stability, and sustainable development of the ecological environment, which has attracted great attention from all countries in the world [10–12].

At present, the area of land affected by mining in China is about 30,300 km^2, and is increasing at about 700 km^2/a. The subsidence area of some mining cities exceeds 10% of the total urban area. With the proposal of the carbon neutral and carbon peak strategy, and the acceleration of urbanization process, the contradiction between the increasing subsidence area and the tension of construction land has become increasingly prominent, which has become one of the main problems limiting the integrated development of urban and rural. Due to the tight land supply, it is inevitable to carry out ecological restoration or engineering construction in the subsidence area [13–15], and even to build subways, high-speed railways, which indicating that subsidence area are no longer abandoned land, but a valuable resource to be developed [16]. However, abandoned goaf may be activated under additional stress and induce secondary damage [17–20], such as the collapse of the Fengfeng Group Machinery Plant, which was built above the abandoned area after 20 years. Therefore, whether the subsidence area can be used as construction land depends on the control of surface residual deformation, and the effectiveness of surface residual deformation control depends on its formation mechanism.

In terms of surface residual deformation characteristics and prediction, Goulty concluded that surface subsidence has different mechanical mechanisms during the active and residual deformation stages, and is not possible to predict the residual subsidence time according to the active stage [21]. Guéguen analyzed the average surface residual deformation of abandoned goaf in northern France as 10 mm/a within 7 years after stopping mining [22]. Statham analyzed the collapse accidents of 400 abandoned goaf in South Wales, and 16% were caused by the buildings stress [23]. Meanwhile, Graniczny [24], Blachowski [25], and André [26] et al. have continuously monitored the surface residual deformation of the abandoned goaf and obtained the residual subsidence in the corresponding time period. In terms of the prediction of surface residual deformation, Cui established a model to calculate the duration of residual subsidence and the annual residual surface subsidence factor caused by abandoned longwall coal mining [27]. Li proposed a novel mathematical model calculating surface progressive residual subsidence based on the logistic time function [28]. Meanwhile, many scholars [29–32] have established prediction models for surface residual deformation under the different mining conditions based on the probability integral method, and have successfully carried out field. Due to the difference geological conditions leads to different degrees of surface residual deformation, based on the overburden failure degree and regional division of mining fracture, this paper analyzes the generation mechanism of surface residual deformation from the source of underground mining, providing a theoretical basis for effective control of surface residual deformation and rational use of abandoned goaf land.

2. Surface Subsidence Characteristics under the Mining Influence

2.1. Overview of the Study Area

Xinlong Mining Co., Ltd. is located 6.0 km southwest of Yuzhou City, China, the coalmine is delineated by 28 coordinated inflection points, which is 8.5~13.4 km long from east to west, 4.5 km wide from south to north, and covers an area of 43.8 km^2. The north and east are slightly inclined plains in front of mountains, with flat terrain, densely distributed villages, and ground elevation of +105~+120 m. The west and south are hills, and the ground elevation gradually decreases from west (+325 m) to east (+105 m). The designed production is 0.9 Mt/a, the mining thickness of No. 21 coal seam is about 4.5 m, the mining depth is 424~634 m, and the dip angle is 5~18°. At present, the 11 mining area has been

completed, the panel distribution and its mining time in the west wing of 11 mining area are shown in Figure 1.
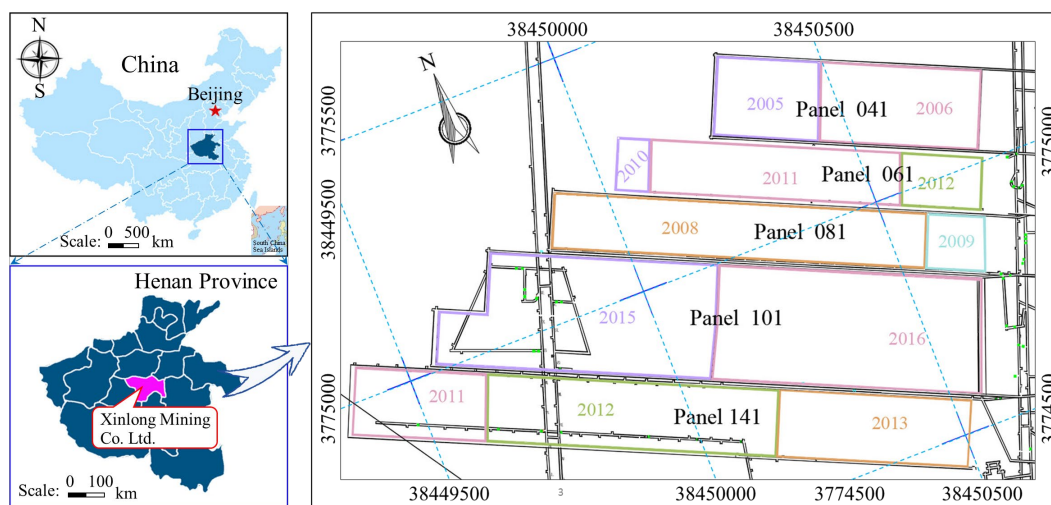

Figure 1. The panel distribution and its mining time of the west wing in the 11 mining area.

As can be seen from Figure 1, the mining time of panel 141 and 061 are basically same, but the boundary conditions are different, where the panel 141 has coal pillars. The strike is 1263 m and the dip is 136 m. The average mining depth is 580 m, with an average of 12°. In general, the coal seam in the middle and west of the coalfield are relatively thick and slightly thin on both sides. The proctor hardness $f = 0.15 \sim 0.25$, which is an extremely soft coal seam. Both sides of the panel 061 are goaf, with strike length of 747.8 m and average dip length of 112.3 m. The coal thickness is 2.6~5.3 m, and 8~12° of dip, and the whole working face is typically thicker in the middle and west, and slightly thinner on both sides. The roof of the working face is relatively hard, and full caved management is adopted.

2.2. Surface Response Characteristics under the Mining Influence

In combination with the mining time of each working face, an observation line with a spacing of 30 m is arranged on the strike and dip of panel 141 and 061, respectively. The observation time of 141 working faces is from November 2011 to March 2014, nine leveling surveys and four comprehensive observations were carried out. The observation time of panel 061 is from September 2011 to October 2012, during which eight leveling surveys were conducted. The strike subsidence curve is shown in Figure 2 based on the monitoring data.

It can be seen from Figure 2 that the maximum subsidence of the two panels are 153 mm and 1632 mm, respectively, which is mainly because the strike and dip of the 061 working face have reached critical mining under the influence of adjacent goaf. The overburden separation and fractures have been fully developed, broken rock in the caved zone has been compacted, and the overburden void is relatively small. The cracks and subsidence occurred on the surface during the mining process, which continued to extend forward with the mining progress. Meanwhile, the structure cracks were caused at the upper corner of the window (as shown in Figure 3). It indicates that when the working face is sub-critical mining, the surface still has large subsidence under the mining influence of the adjacent panel, which will cause serious damage to the surface.
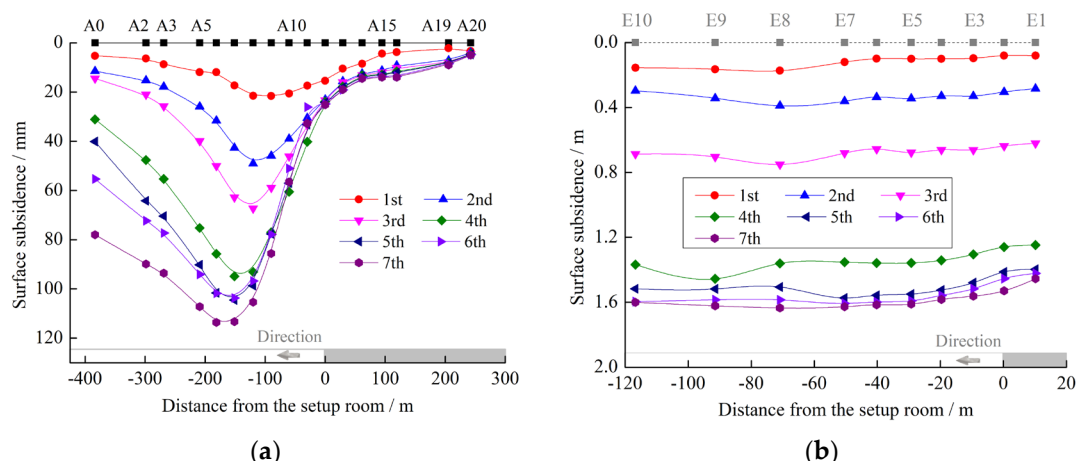
Figure 2. The surface subsidence of the working face in the 11 mining area: (**a**) surface subsidence of panel 141, and (**b**) surface subsidence of panel 061.
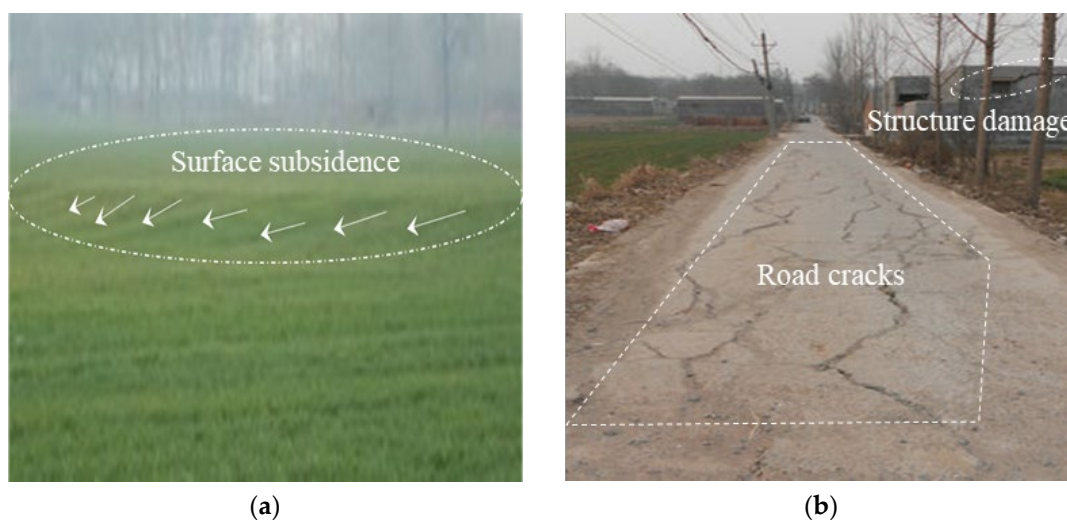

Figure 3. The response of surface and structure under the mining influence: (**a**) surface subsidence and (**b**) surface and structure damage.

3. Overburden Failure Characteristics

The overburden structure is an important basis for maintaining the overburden stability. During the mining process, the overlying strata collapses. When the roof is pressed periodically, the stress and fracture of the collapsed rock will change again. The final manifestation is that there are significant differences in the overburden structure at the open cut, middle area and stopping line of the goaf. Therefore, it is necessary to analyze the distribution characteristics of the stress and overburden fractures after mining.

3.1. Numerical Simulation

Based on geological and mining conditions and borehole histogram of 11,061 working face, 3DEC is adopted to establish the length, width, and height of a 230 m × 210 m × 120 m three-dimensional numerical model, the overburden thickness of the simulated working face is 94.11 m and applied the unstimulated 380 m rock stratum load 9.38 MPa above the model. The Mohr-Coulomb criterion is selected as the constitutive model, and the area contact elastoplastic model is selected as the joint constitutive model. The physical and mechanical parameters of partial strata are shown in Table 1, and the stress distribution of mining overburden at different advanced distances is shown in Figure 4.

Table 1. The physical and mechanical parameters of partial overburden above the working face.

No.	Lithology	Thickness (m)	Elastic Modulus (GPa)	Tensile (MPa)	Poisson's Ratio	Cohesion (MPa)	Friction Angle (°)
1	Sandstone	10.3	10.9	1.68	0.23	1.05	30
2	Sandy mudstone	3.0	14.5	3.05	0.27	1.18	32
3	Medium sandstone	0.9	36.1	5.13	0.26	4.40	36
4	Mudstone	7.7	14.5	3.05	0.27	1.18	32
5	Medium sandstone	3.2	36.1	5.13	0.26	4.40	36
6	Sandy mudstone	2.5	14.5	3.05	0.27	1.18	32
7	Mudstone	1.3	6.9	1.68	0.23	1.05	30
8	Siltstone	1.3	21.6	3.84	0.20	2.75	38
9	Mudstone	2.9	6.9	1.68	0.23	1.05	30
10	Sandy mudstone	1.3	14.5	3.05	0.27	1.18	32
11	Mudstone	8.7	6.9	1.68	0.23	1.05	30
12	Siltstone	1.1	21.6	3.84	0.20	2.75	38
13	Mudstone	8.9	6.9	1.68	0.23	1.05	30
14	Medium sandstone	5.7	36.1	5.13	0.26	4.40	36
15	Sandy mudstone	6.9	14.5	3.05	0.27	1.18	32
16	Mudstone	4.5	6.9	1.68	0.23	1.05	30
17	Siltstone	4.8	21.6	3.84	0.20	2.75	38
18	Mudstone	1.7	6.9	1.68	0.23	1.05	30
19	Sandy mudstone	6.2	14.5	3.05	0.27	1.18	32
20	Fine sandstone	7.6	38.4	6.75	0.18	3.80	37
21	Sandy mudstone	4.7	14.5	3.05	0.27	1.18	32
22	Coal seam	4.5	2.3	1.03	0.31	0.50	24
23	Mudstone	3.8	6.9	1.68	0.23	1.05	30

It can be seen from Figure 4 that with the working face advancing forward, the abutment pressure at the working face boundary is 15.8~29.8 MPa, which is about 2~3 times the original rock stress. The pressure relief area with an arch shape appears in the rock above the working face, and the normal stress phenomenon appears in some overburden near the coal seam, indicating that there is a local tensile stress area in the overburden. When the working face advances 80 m, the pressure relief area reaches the maximum, under the old roof pressure, the local rock strata gradually compact and a compacted area appears. In the process of advancing to 120 m, the pressure relief area is no longer developed upward, while the compacted area continues to expand to the top of the pressure relief area. As the working face continues to advance, there is no obvious change in the range of the relief area at the open cut side, the width of the relief area at the working face side is basically stable and moves with the working face, and the range of compacted area in the middle continues to expand, and the width of the relief area at the open cut side is always smaller than that at the stopping line, which also verifies that the overburden breaking angle at the open cut is greater than that at the stopping line [33]. It can be seen that the overburden in the middle of the goaf is in a compacted state, while the overburden structure exists at the boundary of the working face, indicating that the boundary of the working face is the main area where the overburden voids exist.

In order to further analyze the overburden failure and structural characteristics, combined with the numerical models, the distribution of overburden cracks with different advancing distances was obtained as shown in Figure 5.
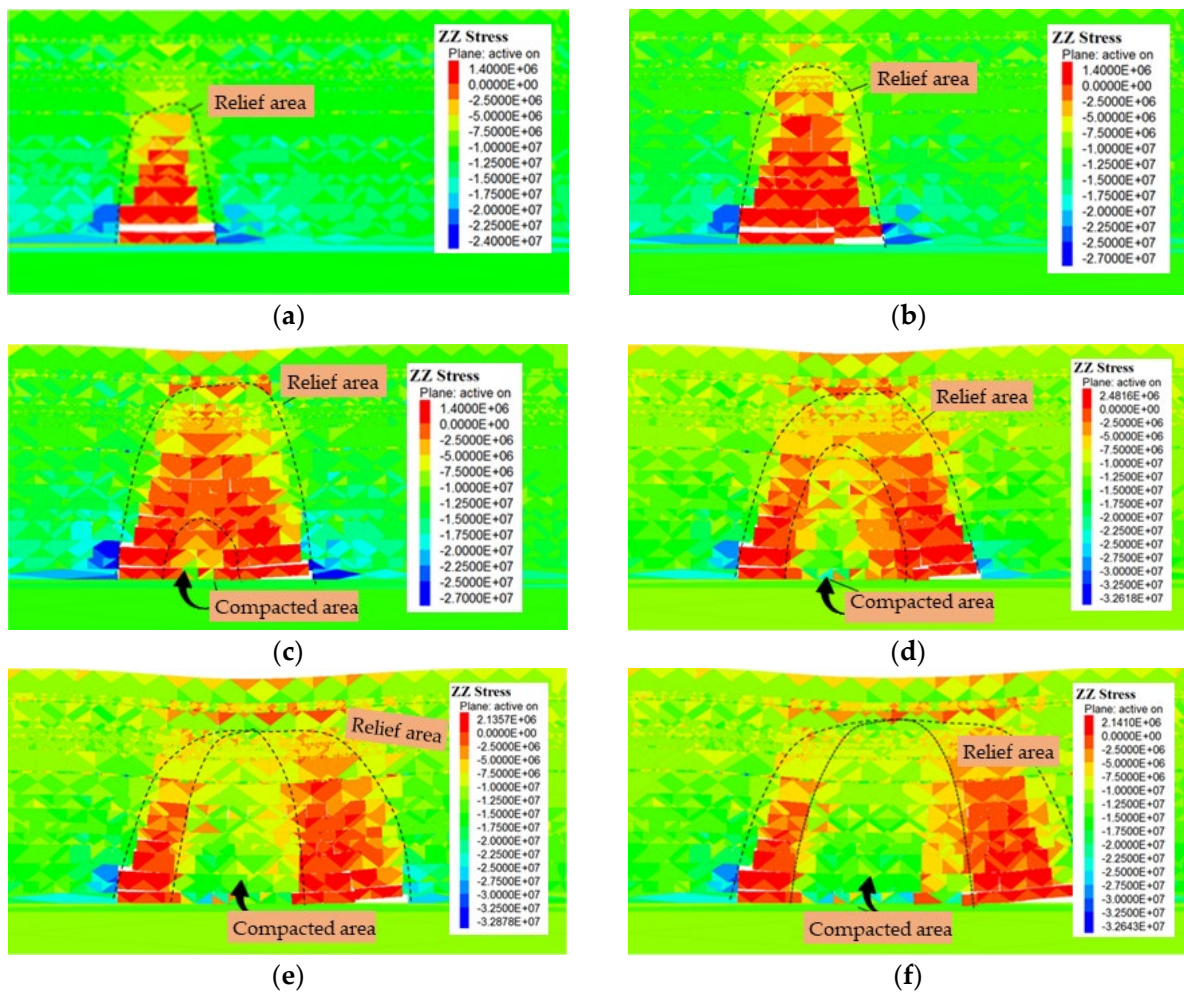
Figure 4. The overburden stress distribution at different advanced distances: (**a**) advance 40 m, (**b**) advance 60 m, (**c**) advance 80 m, (**d**) advance 100 m, (**e**) advance 120 m, and (**f**) advance 140 m.
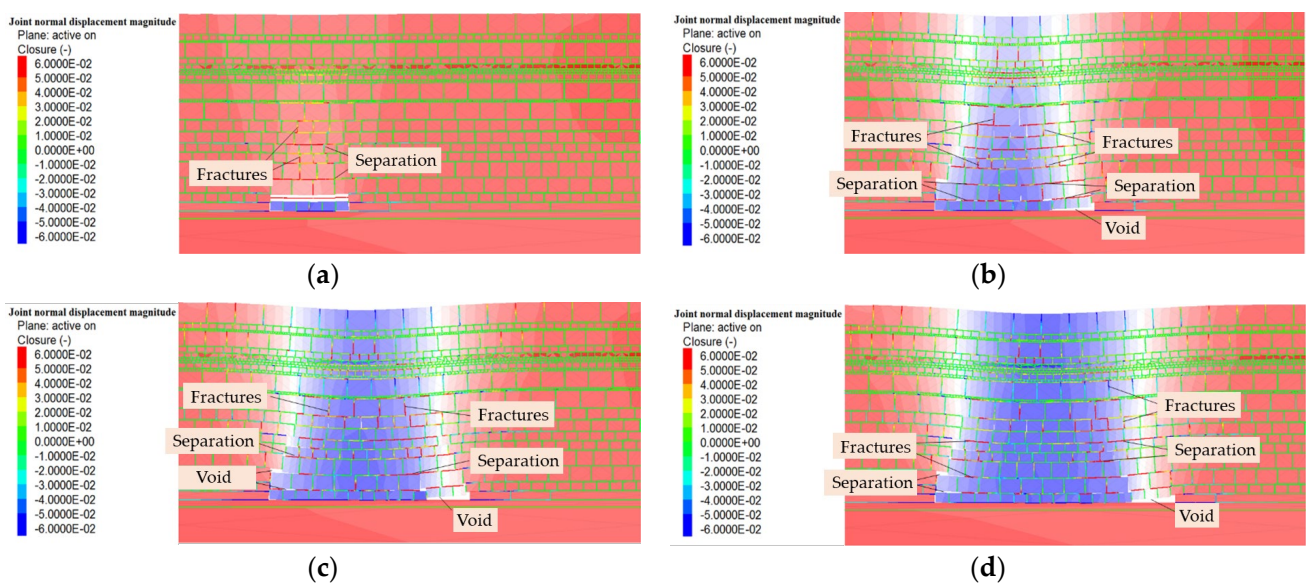

Figure 5. The distribution of overburden cracks with different advancing distances: (**a**) advance 40 m, (**b**) advance 80 m, (**c**) advance 100 m, and (**d**) advance 120 m.

As shown in Figure 5, when the working face advances 40 m, the development height of mining fractures and separation layers is about 18 m, the separation layers are mainly formed due to the asynchronous movement of the rock stratum, and the mining fractures are formed by the fracture of the rock stratum. When advancing 80 m, the separation layer and fractures develop upward, and the fractures develop to 36.4 m, while the separation layer is about 63 m, the cracks in the overburden rock under mining develop upward in a trapezoidal manner, the separation layer develops upward in an inverted trapezoidal manner, and the cracks closure phenomenon appears in the middle goaf. When advancing 100 m, the height of fracture development remains unchanged, indicating that the height of the fracture zone reaches the maximum, while the separation layer continues to develop upward to 74 m. Due to the existence of overburden structure, the side cracks of the open cut are basically unchanged, and the side cracks of the working face move forward continuously. When the panel advances 120 m, the compaction area in the middle goaf increases continuously, and the range of fracture development area on the working face side is larger than that on the open cut side.

From the evolution of mining cracks, it can be seen that the cracks in the middle of the extraction area gradually close after compaction and the area range keeps expanding; due to the existence of a masonry beam structure at the boundary, the cracks are well-developed and stable, which also indicates that the movement space after the reactivation of overburden is mainly concentrated in the fractured zone and caved zone.

3.2. Physical Simulation

Based on the geological and mining conditions of the working face, a 1:50 similar model is established using river sand, calcium carbonate, gypsum, and other materials. According to the key strata theory, there are four key strata that were calculated to exist within the overburden rock. Due to the limited size of the test stand, in order to more accurately analyze the migration and fracture evolution of mining overburden, a 1:50 similarity ratio was selected based on the test-bed size ($2500 \times 200 \times 1300$ mm), and the similarity scale coefficient of the physical model as shown in Table 2 [34].

Table 2. Similarity scale coefficient of physical model.

Category	Geometric Ratio	Time Ratio	Density Ratio	Strength Ratio	External Force Ratio	Elastic Modulus Ratio	Poisson's Ratio
Coefficient	1/50	1/10	0.6	0.012	1.2×10^{-6}	0.012	1

Due to the burial depth of coal seam is too large, the model was not simulated to the surface, and the remaining overburden was applied to the top of the model with an equivalent load of 0.18 MPa. Therefore, this overburden has only three inferior key strata in the model, nine equidistant measuring lines are laid on the model, all measuring points are 10 cm apart, and 225 non-coding points are arranged. Combined with the actual mining speed of the panel (6.7 m/d) and the similarity scale coefficient of physical model, the model is advanced at a speed of 10 cm/1.8 h from the right side. The overburden failure characteristics and its structural evolution are shown in Figure 6.
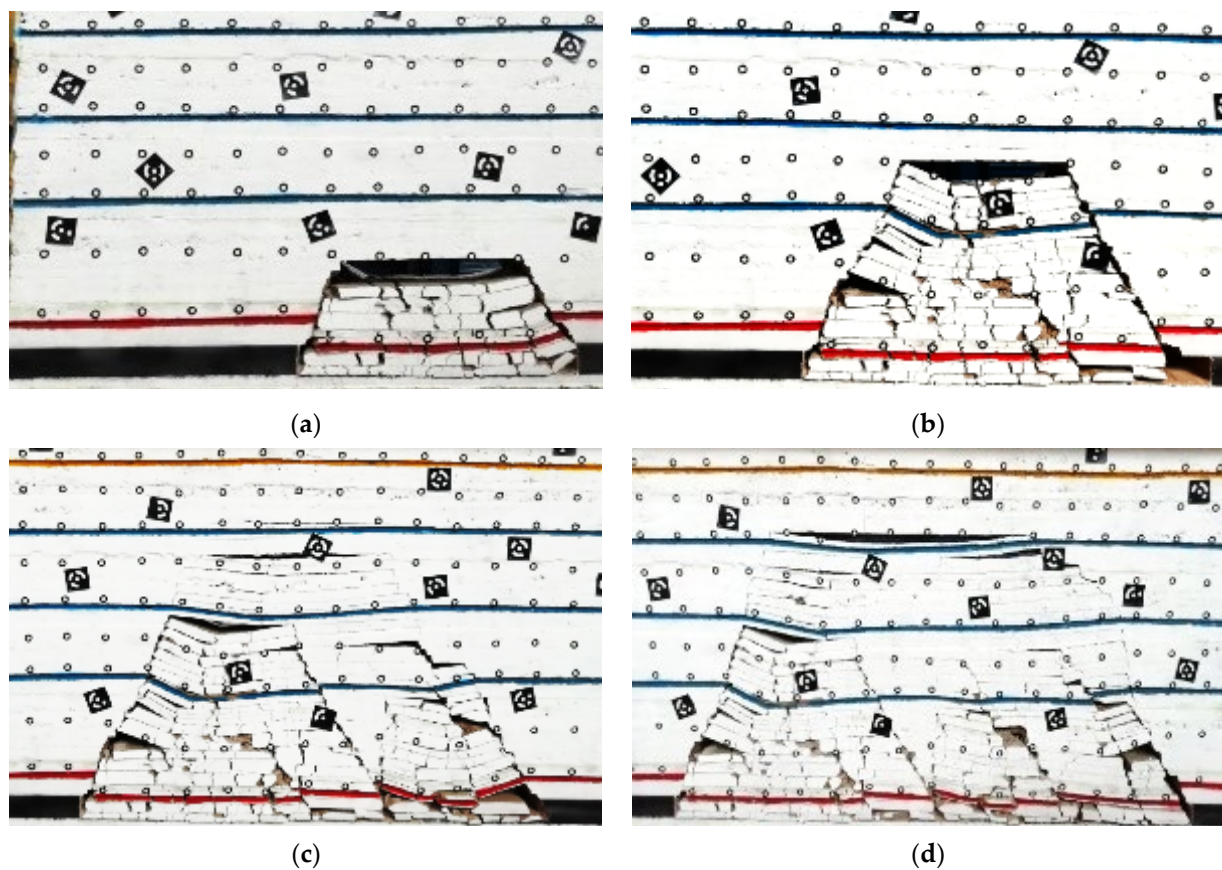
Figure 6. The failure characteristics and evolution of the overburden structure: (**a**) advance 30 m, (**b**) advance 45 m, (**c**) advance 61 m, and (**d**) advance 78.5 m.

From Figure 6, it can be seen that when the face has advanced 30 m, the height of the caved zone of the overburden rock reaches the maximum, at the meantime, the rock strata in the goaf have no bearing effect and only accumulate in the goaf to form a pressure relief area. When advancing 45 m, the masonry beam structure appears in the overburden at the side of the open cut, at which time the overburden failure enters the crack zone range, and the contact state between the middle of the caved zone and the rock strata above gradually changes from no contact to point-surface, line-surface, and surface-surface contact. When advanced 61 m, a temporary masonry beam structure is formed again at the working face, the separation space of the lower rock strata is compacted, and the separation between the upper rock strata is intensified, meanwhile, the overburden structure on the mining side only shows dynamic evolution, and the change of gap distribution mainly occurs on the fracture side of the panel. When it is advanced to 78.5 m, the mining fractures develop below the sub-key stratum, the overburden failure height reaches the maximum, and the breaking angle of the rock stratum at the mining side is smaller than that at the open cut side with distributed asymmetrically. The rock stratum in the middle goaf forms a compacted area due to the closure of the gap, while the two ends of the goaf present a pressure relief area due to the overburden structure. Therefore, when the working face reaches critical mining, the overburden failure height reaches the maximum. The rock stratum gap in the middle of the fracture zone is gradually compacted, and the overburden failure height at goaf boundary and the caved zone in the middle is the main areas where the overburden gaps exist.

4. Mechanism and Discussion of Surface Residual Deformation in Abandoned Goaf

4.1. Influence Factors

The formation of surface residual deformation mainly lies in the overburden gaps, and the distribution of overburden gaps mainly lies in the overburden failure and its structure [35]. Thus, the influencing factors of surface residual deformation are equivalent to that of overburden structure and caved zone, which also is the influence factors of overburden failure height.

1. Overburden lithology: When the overburden is of hard lithology, it is easy to produce fracture and break under the influence of mining, and the overburden failure height is large. Conversely, when it is a soft lithology, the rock stratum is not easy to break and the failure height of the overburden formed by it is small. In addition, it is known from the empirical formula in the Specification that the calculation of the height of the caved zone and fracture zone under the same mining conditions is based on the overburden lithology as an indicator.

2. Coal seam occurrence state: It primarily includes coal seam dip angle, buried depth, etc. The larger the coal seam dip angle is, the saddle shape of overburden failure will gradually change into a parabola shape, which is mainly due to the gradual increase of the tangential sliding force of the overburden along the bedding plane, while the pressure acting on its level becomes smaller, and the broken rock block in the goaf moves downward results in the space above is larger than that below. The influence of coal seam burial depth on overburden failure is mainly reflected in the severity of overburden failure.

3. Roof control methods: It is equivalent to the mining method and determines the overburden failure height, mainly including four types: full collapse, full filling, partial filling, and coal pillar support. When the full caving method is used to manage the roof, the overburden caving is the most sufficient and the failure height is the largest; while for roof management with the full filling method, based on the principle of equivalent replacement, the limited collapse space of the rock stratum results in a small overburden failure height, which is an effective measure to reduce the failure height of overburden, and also a technology to restrain mining disturbance from the source.

4. Mining thickness: It is the main factor affecting the maximum height of overburden failure in high-strength mining. In general, the greater the mining thickness of the coal seam, the larger the space for the collapse of the overlying strata, the higher the height of the water-conducting fracture zone of the rock stratum, and the larger the range of the overburden gaps and mining fractures, thus the potential for the residual deformation of the goaf surface is also increased.

5. Working face size: The smaller values of strike and dip length determine the overburden failure height. When the dip of the working face does not reach full mining, the overburden failure height will increase with the increase of the dip length, and will not be affected by the mining size when it reaches the maximum; only when the size of the working face meets the requirements of full mining, the overburden failure height reaches the maximum value under the geological conditions, and the residual deformation of the goaf surface will also reach the maximum.

6. Advancing speed: The fast-advancing speed of the working face is one of the factors inducing roof disaster. Since the overburden cannot be fully depressurized in a short time, the integrity of the rock stratum after destruction is strong and the gap formed after accumulation in goaf is small. The range of the overburden pressure relief area and adjacent failure area decreases with the increase in work speed. On the contrary, when the advancing speed is low, the scope of overburden failure will increase, thus forming more overburden gaps. For the residual deformation of abandoned goaf, it is also equivalent to the influence of mining time.

In summary, the main factors affecting the residual deformation of goaf are overburden lithology, coal seam occurrence, mining method, mining thickness, working face size, and advancing speed. The influencing factors all affect the residual deformation of the goaf through the height of the fracture zone or the overburden structure, while the residual deformation of the goaf is closely related to the overburden gaps. Since the overburden gaps are mainly concentrated in the fracture zone on both sides of the goaf and the caved zone in the middle, it is necessary to study the compaction deformation characteristics of the broken rock in the caved zone.

4.2. Compaction Characteristics and Discussion of Broken Rock

Combined with the geological conditions of the mine, the sandstone of the caved zone was selected to carry out the compaction deformation test of the broken rock. The test mainly analyzes the influence of particle size, gradation combination, and saturated state on the deformation of broken rock from the perspective of stress-strain, providing a theoretical basis for the formation mechanism and prevention and control ideas of surface residual deformation in abandoned goaf.

4.2.1. Experiment Scheme

The physical and mechanical parameters are tested by processing the test rock sample into a standard sample, and the mechanical parameters are shown in Table 3.

Table 3. Standard physical parameters of sandstone.

Density (g·cm^{-3})	Elastic Modulus (GPa)	Tensile (MPa)	Poisson's Ratio	Friction Angle (°)
2.49	24.9	5.68	0.25	32.4

Crushed stone with a particle size of 0~10 cm is used in the test, and five groups of particle size samples with the particle size of 0~2 cm, 2~4 cm, 4~6 cm, 6~8 cm, and 8~10 cm are sieved, respectively. Crushed rock deformation seepage test system is used to conduct crushed rock compression test. The inner diameter of the test cylinder is 400 mm, the cylinder height is 680 mm, the material is 45 # steel, and the displacement and stress dual control servo loading system is used to achieve dual control of displacement and stress. The test is divided into four groups, with a loading rate of 0.5 kN/s and a load application range of 0~450 kN. The specific scheme is as follows:

(1) The first group mainly studies the pressure-bearing deformation of five groups of broken rock with different particle sizes (0~2 cm, 2~4 cm, 4~6 cm, 6~8 cm, 8~10 cm) under dry and continuous loading.

(2) The second group mainly studies the pressure-bearing deformation of seven groups of broken rock with different grading indexes (n = 0.2~0.8) under dry and continuous loading.

(3) The third group mainly studies the influence of saturated water on the pressure-bearing deformation of broken rock when the gradation index n = 0.2.

Place each group of crushed stones in the test cylinder one by one, so that their natural stacking height is close to 32 cm, and the error between each group is not more than 0.5 cm. The natural stacking height and amount of each group of crushed stones in the test are shown in Table 4.

Table 4. The accumulation parameters of broken rocks with different particle sizes.

No.	Particle Size (cm)	Stacking Height (cm)	Mass (g)	Volume (cm³)	Density (g·cm⁻³)
1	0~2	32.28	56,338	40,539.92	1.389692
2	2~4	32.11	51,246	40,317.83	1.271051
3	4~6	32.07	47,775	40,277.54	1.186145
4	6~8	32.26	46,387	40,508.67	1.145113
5	8~10	31.91	45,568	40,068.75	1.137245

4.2.2. Results and Discussion

1. Different particle sizes

Using the displacement-stress dual control servo system, the dry crushed stone in the test cylinder is loaded step by step, and the application of axial load and the change of crushed stone displacement with time is recorded in real-time. The stress-strain relationships for the five groups of grain-size crushed stones are shown in Figure 7.
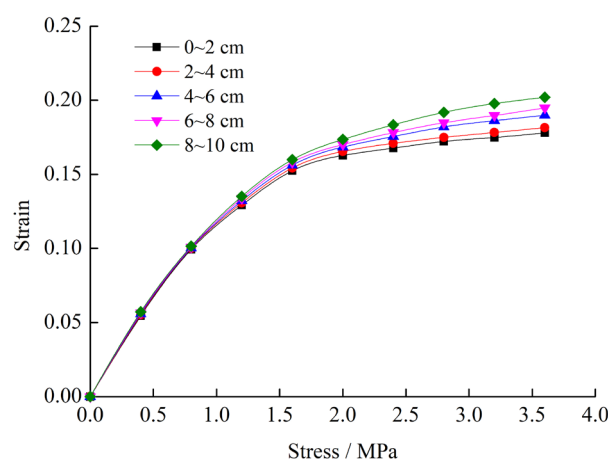
Figure 7. The stress-strain for sandstone with different particle sizes.

It can be seen from Figure 7 that the strain increase rate of the five groups of particle-size crushed stone in the low-stress stage is greater than that in the high-stress stage. At the initial stage, the contact mode between crushed stone particles is mainly point-point, which makes up a very loose skeleton with a large gap size, and connectivity between gravel particles is good, and the deformation develops rapidly. With the increase of stress, a part of crushed stone is compressed and deformed or even broken, small particles fill the gaps to form a more compact structure, and the contact gradually transits from point-point contact to point-face and face-face contact. Meanwhile, the ability of a crushed stone to resist deformation gradually increases, so the strain increases rate in the low-stress stage is greater than that in the high-stress stage.

2. Different gradations

Using the Talbol grading theory was used for the particle size proportioning of different graded crushed stones, and the mass of each group of graded aggregates was specified to be 50 kg, and the continuous loading test of 0~450 kN is carried out for 4 groups of graded crushed stones under different grading indexes. The stress-strain curve of each group of graded crushed stones is shown in Figure 8.
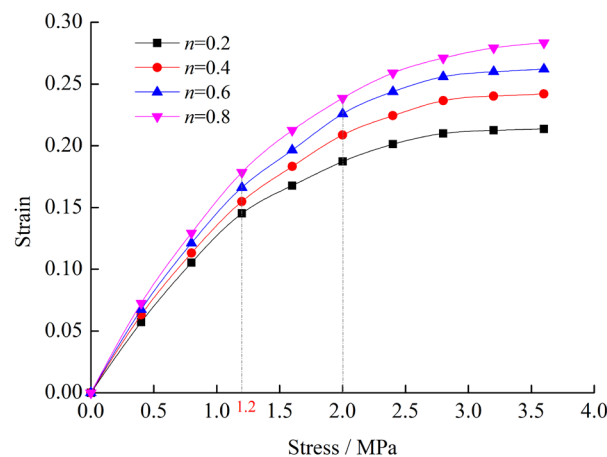
Figure 8. The stress-strain for sandstone with different grading indexes.

It can be seen from Figure 8 that at the initial stage of stress application, the strain of broken rocks in each group of graded increases rapidly under different gradation indexes. When the stress exceeds 1.2 MPa, the strain of crushed stone rises slowly, and the strain gap between each group of crushed stone becomes larger, mainly due to a large number of gaps between different particle sizes of crushed stone, which is easy to deform under stress, and the crushed stone gap is compressed to form. When the stress is greater than 2.0 MPa, the strain gap of each group of the crushed stone changes obviously, mainly because the proportion of large-size crushed stone increases with the increase of grading index, and the porosity is easier to compact with the rise of gradation index, the edges of large-size broken rocks grind each other and become smooth, and the generated small size rock blocks fill the gaps of the rock blocks. Therefore, the crushed stone group with index n has a relatively sizable final strain value.

3. Water-saturated graded broken sandstone

Put the crushed sandstone (50 kg) with n = 0.2 into the test cylinder for a water-saturated compaction test, so that the internal pores of the crushed stone are filled with water. By comparing with the stress-strain relationship of dry broken rock under continuous loading, the results are shown in Figure 9.
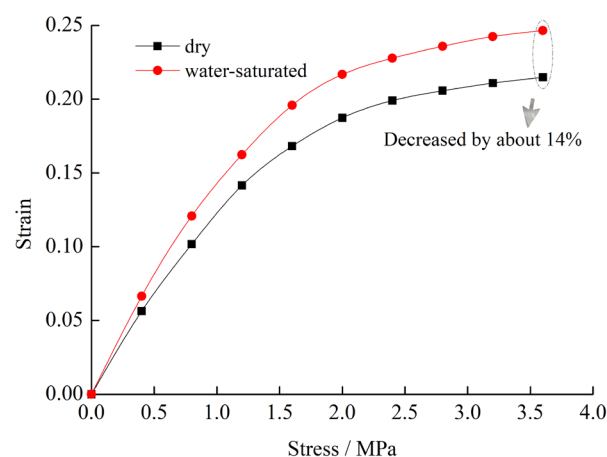

Figure 9. The stress-strain of dry and water-saturated sandstone samples.

As shown in Figure 9, the strain of water-saturated crushed stone under the same stress is obviously greater than that under the dry state. It is mainly because the water weakens the cohesion between the rock particles, water molecules reduce the connection between the internal particles of the rock sample so that the energy required for rock fracture is

reduced, the strength of the crushed stone is diminished, and deformation is more likely to occur under load. Meanwhile, large size crushed stone will be broken into smooth particles again and fill the gap again so that the rock strain increases. In addition, the bearing capacity of broken sandstone is reduced by nearly 14% under the water-saturated influence, which indicates that the water content has a significant impact on the compaction of broken sandstone.

In summary, the compaction of broken rocks in the caved zone is the main factor that causes residual surface deformation in the middle of the goaf, and it is also one of the factors that affect the stability of the overburden structure on both sides of the goaf. It can be seen that the formation mechanism of the surface residual deformation is mainly due to the overburden structure on both sides of the goaf and the compaction of the broken rocks in the caved zone, and the surface shows that the residual subsidence on both sides of the goaf is slightly greater than that in the middle of the goaf.

5. Engineering Applications

Due to the mining time of the west wing of 11 mining area is from 2005 to 2016, the surface will enter a recession period within 2.5–3 years after mining. Therefore, the goaf has entered the stage of surface residual deformation. By setting up a control monitoring network with a spacing of 50×100 m above the abandoned goaf, a total of 3 (6 sections) observation lines are arranged in a grid-like, and named line A, line B, and line C, respectively. There are 127 measuring points for Line A, 72 measuring points for Line B and 153 measuring points for Line C. By using RTK monitoring technology of the level D horizontal control network, the surface residual deformation of each measuring point from February 2019 to August 2022 were obtained. The measuring points in the west wing of 11 mining area and its residual subsidence are shown in Figure 10.
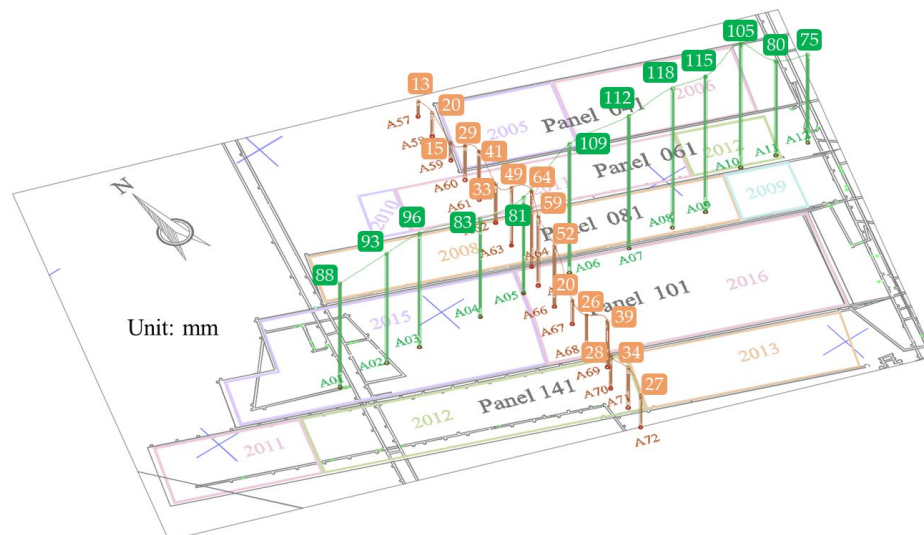

Figure 10. The measuring points and its residual subsidence in the 11 mining area.

As shown in Figure 10, the maximum residual deformation value of A8 is 118 mm, which is located between 101 and 081 working faces. This is mainly due to the late mining time of the 101 working face and the secondary activation of mining overburden rock caused by repeated mining. It also verifies the accuracy that the overburden gaps are mostly concentrated at the overburden structure. In addition, the measuring subsidence at the boundary of the goaf is basically greater than that in the middle goaf, which also further verifies that the gaps on goaf boundary are more than that in the middle goaf. Based on the subsidence curve on the dip, the cumulative subsidence of the measuring point generally shows a change law of first increasing and then decreasing, which is mainly caused by the different mining time. The subsidence curve presents a wave state after passing through

A68, mainly caused by the different positions of measuring points and goaf. It shows that the gap compression at the overburden structure is greater than that at the middle goaf, which again verifies the previous conclusion above. In conclusion, the surface residual deformation above the goaf is closely related to the mining time. The later the mining is completed, the greater the cumulative subsidence of surface residual. For the old goaf (such as the panel 041) that has been mined for more than 15 years, the surface residual deformation is basically 15~20 mm/a, which indicates that surface residual deformation has a long-term characteristic, and the measures should be taken to reduce the generation of residual deformation during the surface utilization above the abandoned goaf.

6. Conclusions

1. Based on the surface response characteristics under the influence of mining, the characteristics of trapezoidal and periodic forward movement of overburden failure during mining were analyzed, and the transmission law of mining fracture up layer by layer with the overburden failure was studied, and the overburden structure was formed at the steep subsidence curve was clarified.
2. The main influencing factors of surface residual deformation in abandoned goaf were analyzed, and the characteristics of broken rock in the caved zone under different conditions (particle size, grading, and water content) were studied and the overburden structure on both sides of the goaf and the compaction of the caved zone where the formation mechanisms of surface residual deformation was revealed.
3. The field-measured data show that the surface subsidence near the goaf boundary was greater than that in the middle goaf, the correctness of the overburden voids distribution and the source of residual deformation in goaf was verified. Meanwhile, the surface residual deformation has long-term and dangerous characteristics were analyzed, which provides a theoretical basis for scientific prevention of the surface residual deformation and the effective utilization of the mining subsidence area.

References

1. Bloch, H.; Rafiq, S.; Salim, R. Coal consumption, CO_2 emission and economic growth in China: Empirical evidence and policy responses. *Energy Econ.* **2012**, *34*, 518–528. [CrossRef]
2. Lin, B.Q.; Liu, J.H. Estimating coal production peak and trends of coal imports in China. *Energy Policy* **2010**, *38*, 512–519. [CrossRef]
3. Bai, E.H.; Guo, W.B.; Tan, Y. Negative externalities of high-intensity mining and disaster prevention technology in China. *Bull. Eng. Geol. Environ.* **2019**, *78*, 5219–5235. [CrossRef]
4. Bell, F.G.; Stacey, T.R.; Genske, D.D. Mining subsidence and its effect on the environment: Some differing examples. *Environ Geol.* **2020**, *40*, 135–152. [CrossRef]

5. Sun, Q.; Zhang, J.X.; Li, M.; Zhou, N. Experimental evaluation of physical, mechanical, and permeability parameters of key aquiclude strata in a typical mining area of China. *J. Clean. Prod.* **2020**, *267*, 122109. [CrossRef]

6. Karakus, M.; Tutmez, B. Fuzzy and multiple regression modelling for evaluation of intact rock strength based on point load, schmidt hammer and sonic velocity. *Rock Mech. Rock Eng.* **2006**, *39*, 45–57. [CrossRef]

7. Jing, Z.R.; Wang, J.M.; Zhu, Y.C.; Feng, Y. Effects of land subsidence resulted from coal mining on soil nutrient distributions in a loess area of China. *J. Clean. Prod.* **2018**, *177*, 350–361. [CrossRef]

8. Booth, C. Groundwater as an environmental constraint of longwall coal mining. *Environ. Geol.* **2006**, *49*, 796–803. [CrossRef]

9. Salmi, E.F.; Nazem, M.; Karakus, M. Numerical analysis of a large landslide induced by coal mining subsidence. *Eng. Geol.* **2017**, *217*, 141–152. [CrossRef]

10. Liu, J.G.; Diamond, J. China's environment in a globalizing world. *Nature* **2005**, *435*, 1179–1186. [CrossRef]

11. Shahbaz, M.; Nasir, M.A.; Hille, E.; Mahalik, M.K. UK's net-zero carbon emissions target: Investigating the potential role of economic growth, financial development, and R&D expenditures based on historical data (1870-2017). *Technol. Forecast. Soc. Chang.* **2020**, *161*, 120255. [CrossRef]

12. Tajdu's, K.; Sroka, A.; Misa, R.; Hager, S.; Rusek, J.; Dudek, M.; Wollnik, F. Analysis of mining-induced delayed surface subsidence. *Minerals* **2021**, *11*, 1187. [CrossRef]

13. Cui, C.Q.; Wang, B.; Zhao, Y.X.; Xue, L.M. Waste mine to emerging wealth: Innovative solutions for abandoned underground coal mine reutilization on a waste management level. *J. Clean. Prod.* **2020**, *252*, 119748. [CrossRef]

14. Li, L.; Wu, K.; Zhou, D.W. Evaluation theory and application of foundation stability of new buildings over an old goaf using longwall mining technology. *Environ. Earth Sci.* **2016**, *75*, 763. [CrossRef]

15. Yuan, L.; Jiang, Y.D.; Wang, K.; Zhao, Y.X.; Hao, X.J.; Xu, C. Precision exploitation and utilization of closed/abandoned mine resources in China. *J. China Coal Soc.* **2018**, *43*, 14–20. [CrossRef]

16. Lyu, X.; Yang, K.; Fang, J.J. Utilization of resources in abandoned coal mines for carbon neutrality. *Sci. Total Environ.* **2022**, *822*, 153646. [CrossRef]

17. Wang, C.H.; Lu, Y.; Qin, C.R.; Li, Y.Y.; Sun, Q.C.; Wang, D.J. Ground disturbance of different building locations in old goaf area: A case study in China. *Geotech. Geol. Eng.* **2019**, *37*, 4311–4325. [CrossRef]

18. Han, C.P.; Zu, F.J.; Du, C.; Shi, L. Analysis of excavation stability and reinforcement treatment of the cutting slope under the influence of old goaf. *Appl. Sci.* **2022**, *12*, 8698. [CrossRef]

19. Li, P.X.; Yan, L.L.; Yao, D.H. Study of tunnel damage caused by underground mining deformation: Calculation, analysis, and reinforcement. *Adv. Civ. Eng.* **2019**, *2019*, 4865161. [CrossRef]

20. Mhlongo, S.E.; Amponsah-Dacosta, F. A review of problems and solutions of abandoned mines in South Africa. *Int. J. Min. Reclam. Environ.* **2016**, *30*, 279–294. [CrossRef]

21. Goulty, N.R.; Al-Rawahy, S.Y.S. Reappraisal of time-dependent subsidence due to longwall coal mining. *Q. J. Eng. Geol.* **1996**, *29*, 83–91. [CrossRef]

22. Guéguen, Y.; Deffontaines, B.; Fruneau, B.; AlHeib, M.; Michele, M.; Raucoules, D.; Guise, Y.; Planchenault, J. Monitoring residual mining subsidence of Nord/Pas-de-Calais coal basin from differential and Persistent Scatterer Interferometry (Northern France). *J. Appl. Geophys.* **2009**, *69*, 24–34. [CrossRef]

23. Statham, I.; Treharne, G. Subsidence due to abandoned mining in the South Wales coalfield, UK: Causes, mechanisms and environmental risk assessment. In Proceedings of the 4th International Conference on Land Subsidence, Houston, TX, USA, 12–17 May 1991.

24. Graniczny, M.; Colombo, D.; Kowalski, Z.; Przyucka, M.; Zdanowski, A. New results on ground deformation in the upper silesian Coal Basin (southern Poland) obtained during the DORIS Project (EU-FP 7). *Pure Appl. Geophys.* **2015**, *172*, 3029–3042. [CrossRef]

25. Blachowski, J.; Kopeć, A.; Milczarek, W.; Owczarz, K. Evolution of secondary deformations captured by satellite radar interferometry: Case study of an abandoned Coal Basin in SW Poland. *Sustainability* **2019**, *11*, 913. [CrossRef]

26. André, V. Surface movement above an underground coal longwall mine after closure. *Nat. Hazards Earth Syst.* **2016**, *16*, 2107–2121. [CrossRef]

27. Cui, X.M.; Zhao, Y.L.; Wang, G.R.; Zhang, B.; Li, C.Y. Calculation of residual surface subsidence above abandoned longwall coal mining. *Sustainability* **2020**, *12*, 1528. [CrossRef]

28. Li, C.Y.; Ding, L.Z.; Cui, X.M.; Zhao, Y.L.; He, Y.H.; Zhang, W.Z.; Bai, Z.H. Calculation model for progressive residual surface subsidence above mined-out areas based on logistic time function. *Energies* **2022**, *15*, 5024. [CrossRef]

29. Guo, Q.B.; Meng, X.R.; Li, Y.M.; Lv, X.; Liu, C. A prediction model for the surface residual subsidence in an abandoned goaf for sustainable development of resource-exhausted cities. *J. Clean. Prod.* **2021**, *279*, 123803. [CrossRef]

30. Fan, H.D.; Lu, L.; Yao, Y.H. Method combining probability integration model and a small baseline subset for time series monitoring of mining subsidence. *Remote Sens.* **2018**, *10*, 1444. [CrossRef]

31. Sun, Q.; Zhou, N.; Song, W.J.; Zhao, X. Risk assessment and prevention of surface subsidence under buildings by cemented paste filling and strip mining methods: A case study. *Adv. Civ. Eng.* **2021**, *2021*, 9965279. [CrossRef]

32. Vervoort, A. The time duration of the effects of total extraction mining methods on surface movement. *Energies* **2020**, *13*, 4107. [CrossRef]

33. Yu, Q.G.; Zhang, H.X.; Deng, W.N.; Zou, Y.P. Analysis of influencing factors of surface skewed subsidence based on key strata theory. *J. China Coal Soc.* **2018**, *43*, 1322–1327. [CrossRef]

34. Li, H.C. *Similar Simulation Test of Ground Pressure*; China University of Mining and Technology Press: Xuzhou, China, 2017.
35. Bai, E.H.; Guo, W.B.; Tan, Y.; Guo, M.J.; Wen, P.; Liu, Z.Q.; Ma, Z.B.; Yang, W.Q. Regional division and its criteria of mining fractures based on overburden critical failure. *Sustainability* **2022**, *14*, 5161. [CrossRef]